Regulating Functional Groups Enhances the Performance of Flexible Microporous MXene/Bacterial Cellulose Electrodes in Supercapacitors

Yijia Luo,[1,2] Wenxiu Que,[1] Yi Tang,[3] Yunqing Kang,[2] Xiaoqing Bin,[1] Zhenwei Wu,[2] Brian Yuliarto,[4] Bowen Gao,[5] Joel Henzie*,[2] and Yusuke Yamauchi*[6,7,8]*

1. Electronic Materials Research Laboratory, Key Laboratory of the Ministry of Education & International Center for Dielectric Research, Shaanxi Engineering Research Center of Advanced Energy Materials and Devices, School of Electronic Science and Engineering, Xi'an Jiaotong University, No. 28, Xianning West Road, Xi'an, Shaanxi 710049, P. R. China
E-mail: wxque@mail.xjtu.edu.cn (Prof. W. Que)
2. Research Center for Materials Nanoarchitectonics (MANA), National Institute for Materials Science (NIMS), 1-1 Namiki, Tsukuba, Ibaraki 305-0044, Japan
E-mail: henzie.joeladam@nims.go.jp (Dr. J. Henzie)
3. College of Materials Science and Engineering, Xi'an University of Science and Technology, Xi'an, Shaanxi 710054, P. R. China
4. Advanced Functional Materials Laboratory, Engineering Physics Department, Faculty of Industrial Technology, Institut Teknologi Bandung, Indonesia 40132; and Research Center for Nanoscience and Nanotechnology (RCNN), Institut Teknologi Bandung, Indonesia 40132
5. School of Mechanical and Construction Engineering, Taishan University, Tai'an, Shandong 271021, P. R. China
6. Australian Institute for Bioengineering and Nanotechnology (AIBN), The University of Queensland, Brisbane QLD 4072, Australia
7. Department of Materials Process Engineering, Graduate School of Engineering, Nagoya University, Nagoya 464-8603, Japan
8. Department of Chemical and Biomolecular Engineering, Yonsei University, Seoul 03722, South Korea
E-mail: y.yamauchi@uq.edu.au (Prof. Y. Yamauchi)

ABSTRACT: Ultra-thin MXene-based films exhibit superior conductivity and high capacitance, showing promise as electrodes for flexible supercapacitors. This work describes a simple method to enhance the performance of MXene-based supercapacitors by expanding and stabilizing the interlayer space between MXene flakes while controlling the functional groups to improve conductivity. $Ti_3C_2T_x$ MXene flakes are treated with bacterial cellulose (BC) and NaOH to form a composite MXene/BC (A-M/BC) electrode with a microporous interlayer and high surface area (62.47 m^2 g^{-1}). Annealing the films at low temperatures partially carbonizes the BC, increasing the overall electrical conductivity of the films. Improvement in conductivity is also attributed to the reduction of −F, −Cl, −OH functional groups, leaving −Na and −O functional groups on the surface. As a result, the A-M/BC electrode demonstrates a capacitance of 594 F g^{-1} at a current density of 1 A g^{-1} in 3M H_2SO_4, which represents a 2X increase over similarly processed films without BC (309 F g^{-1}) or pure MXene (298 F g^{-1}). The corresponding device has an energy density of 9.63 Wh kg^{-1} at a power density of 250 W kg^{-1}. BC is inexpensive and enhances the overall performance of MXene-based film electrodes in electronic devices. This method underscores the importance of functional group regulation in enhancing MXene-based materials for energy storage.

KEYWORDS: MXene, Bacterial Cellulose, Functional Group Modulation, Composite Film, Supercapacitor

MXenes are an emerging class of two-dimensional (2D) materials that are typically obtained from the MAX parent phase ($M_{n+1}AX_n$) by etching the "A" layer elements (e.g. Al, Si, Ga, Sn, etc.) to obtain 2D nanosheets with the chemical formula: $M_{n+1}X_nT_x$ (n = 1, 2, 3, or 4), where M is an early transition metal, X is carbon and/or nitrogen, and T_x represents surface functional groups (e.g. −OH, =O, −F, −Cl, −Br).[1-3] They have attracted considerable attention for supercapacitor (SC) applications due to their strong hydrophilicity, high electrical conductivity, abundant surface functional groups, large specific surface area, and pseudocapacitive properties.[4, 5] However, pure MXene flakes presently have limited use in SC applications because 2D materials are susceptible to re-stacking due to van der Waals forces, which decreases the interlayer spacing and negatively affects surface area and ion transport. Intercalating materials are introduced to minimize re-stacking by serving as pillars to maintain greater separation between the MXene flakes.[6]

Bacterial cellulose (BC) is an inexpensive one-dimensional (1D) nanomaterial with high stability, tunable pore structure, and good film-forming properties.[7] Numerous studies have shown that integrating BC nanofibers with MXenes can significantly improve the structural stability of MXene-based electrodes. Examples include PPy@PVA/BC/MXene composite aerogels,[8] MXene ($Ti_3C_2T_x$)/cellulose nanofiber/polyaniline films,[9] MXene/SWCNT/cellulose nanofiber aerogel films,[10] CNF/MXene/AgNW films,[11] and polypyrrole@bacterial cellulose/MXene composite films, among others.[12] Introducing a third material with higher electrical conductivity can improve the hybridization of the MXene/BC mixture. Thus ternary modification is more commonly reported but will increase the cost and complexity of the synthesis process compared to binary MXene/BC systems. Improving the electrochemical performance of binary MXene/BC composite films using inexpensive and scalable methods is crucial for their application in flexible energy storage.[13]

In addition, unfavorable surface functional groups (−OH, −F) also hinder the electrochemical properties of MXenes.[14] Treating MXenes with inexpensive alkali reagents

like LiOH, KOH, $Mg(OH)_2$, or NaOH is a straightforward and environmentally friendly strategy to replace −F groups with −OH and cation groups (e.g. −Li, −K, −Mg, −Na). Subsequent annealing transforms −OH into −O, creating an MXene surface predominantly featuring −O and cation groups that improve the mechanical strength and capacitance of the material.[15, 16] The cation also plays an essential role as it enlarges the interlayer space between MXene flakes.[17-20] NaOH is selected as the alkali treatment agent because it is inexpensive,[21, 22] and −Na intercalation agents generate the largest d-spacings (versus Li, K and Mg) in MXenes.[20] Optimal treatment of MXene with NaOH followed by annealing is expected to yield a surface rich in −O and −Na groups.

Herein, we describe a cost-effective and straightforward method to fabricate alkali-treated MXene ($Ti_3C_2T_x$)/bacterial cellulose (A-M/BC) film electrodes, which exhibit improved performance in SCs. The surface functional groups (T_x) of $Ti_3C_2T_x$ MXene are tunable via alkali treatment and subsequent low-temperature annealing. The 1D BC fibrils serve as extended pillars, enhancing the mechanical integrity of the MXene composite and preventing re-stacking. The specific surface area of these MXene-BC composite films is ~2X larger than pure MXene films (62.47 $m^2\ g^{-1}$ versus 33.09 $m^2\ g^{-1}$, respectively), indicating that BC contributes to maintaining the 3D porous structure within the electrodes. During the low-temperature annealing process under an argon (Ar) atmosphere, the BC is partially carbonized, facilitating its hybridization with the MXene surface. This carbonization step increases the graphitic carbon content, creating a porous nanoscale interlayer space that enhances electrolyte ion transport. Moreover, the alkali and annealing processes are effective in reducing less favorable surface functional groups (−OH, −F, −Cl) on MXene, predominantly leaving −Na and −O functional groups on the surface. Optimal BC concentration results in a significantly enhanced capacitance of the MXene-based composite film electrode has a capacitance of 594 F g^{-1} at a current density of 1 A g^{-1} in 3M H_2SO_4 electrolyte, which is 2X larger than pure MXene (298 F g^{-1}) or MXene treated under alkali and annealing but without

BC (309 F g^{-1}). Correspondingly, the film shows an areal capacitance of 874 mF cm^{-2} and a volumetric capacitance of 2186 F cm^{-3} at a current density of 1 A g^{-1}, respectively. This BC-incorporated sample has a capacitance retention of 83.46% after 10,000 charge/discharge cycles at 50 A g^{-1}. The resulting symmetric supercapacitor (SSC) device has an energy density of 9.63 Wh kg^{-1} at a power density of 250 W kg^{-1}.

RESULTS AND DISCUSSION

Figure 1 illustrates the synthesis protocol for fabricating alkali-treated porous MXene/BC composite films. Delaminated-$Ti_3C_2T_x$ MXene flakes were obtained by etching the layered transition metal carbide 3D precursor Ti_3AlC_2 MAX powder (**Figure S1**) with a mixture solution of hydrochloric acid (HCl) and lithium fluoride (LiF), followed by ultrasonic treatment in an ice bath. Typically, the resulting MXene colloidal suspension (0.5 mg mL^{-1}) is dark green (**Figure S2**). Subsequently, a solution containing BC nanofibers (1 mg mL^{-1}) was mixed with the MXene colloidal suspension, followed by the addition of an aqueous NaOH solution (150 mg/mL) to induce flocculation (NaOH: MXene: BC = 10:1:0 to 0.5 w/w). The MXene colloidal suspension flocculated rapidly as NaOH was added due to the change of the pH value,[23] causing −F functional groups to be replaced with −OH groups due to their higher chemical activity.[24] Na^+ further promoted flocculation by helping to screen the repulsive surface charges between MXene flakes.[25] Vacuum-assisted filtration was then used to obtain the MXene/BC self-supporting composite films. Finally, porous A-M/BC flexible films were obtained by annealing at 400°C for 2 hours (h) under an Ar atmosphere. The composite films were named based on their BC concentration from 0 to 50 %, i.e. A-M/BC-0 (0% BC), A-M/BC-0.1, A-M/BC-0.2 and A-M/BC-0.5 (50% BC). In addition, control samples including pristine MXene films (pure MXene), pristine BC films (pure BC), and MXene/BC films (M/BC) were prepared without alkali and annealing steps.

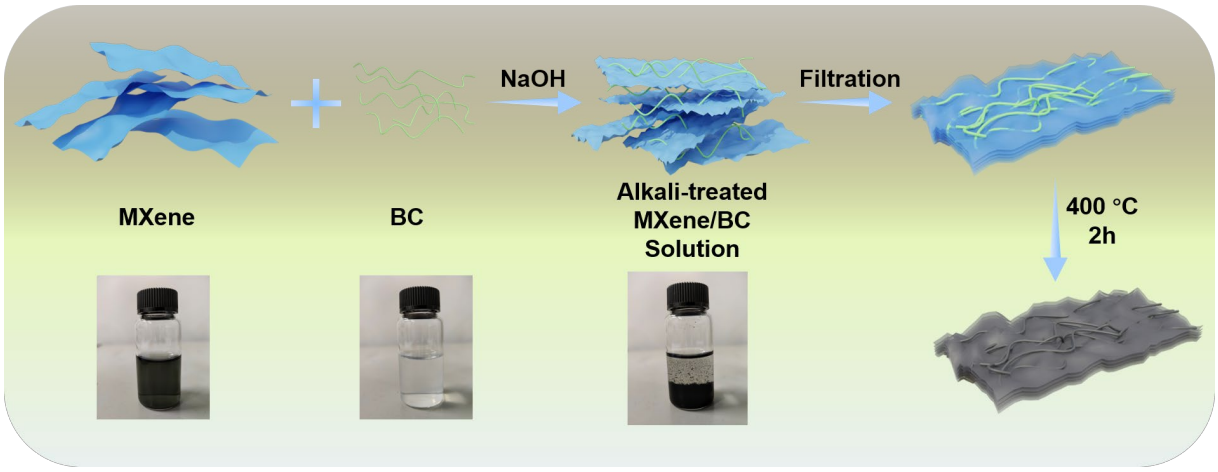

Figure 1. Schematic illustration describing the fabrication of the alkali-treating porous MXene/bacterial cellulose composite films.

According to atomic force microscopy (AFM), the MXene nanoflakes depicted in (**Figure 2a**) are several hundred nanometers (nm) in size and 2.05 nm thick (1−2 layers). The zeta potential of the MXene colloidal suspension is −38.86 mV (**Figure 2b**), which is attribute to the negatively charged −OH, =O, −F functional groups that terminate the MXene surfaces. The zeta potential of the BC nanofiber suspension is −44.47 mV (**Figure 2c**). The greater the absolute value of the zeta potential, the stronger the stability of the solution. The negative zeta potential of BC is higher than that of MXene, indicating that their combination should enhance the stability of the MXene and BC mixture solution. Interestingly, the high negative potential of neat BC suspensions is known to increase film roughness.[26] Regardless, both colloidal sols have high negative zeta potentials, enabling adequate electrostatic repulsion to facilitate conformal hybridization and cross-linking between the BC and MXene flakes as NaOH is added to induce flocculation.

Transmission electron microscopy (TEM) was used to examine the morphological and microstructural changes of the samples after each optimization step. In **Figure 2d,** the TEM image shows that the MXene nanoflakes are extremely thin and almost transparent. The corresponding selected area electron diffraction (SAED) pattern has a hexagonal arrangement of diffraction spots (inset of **Figure 2d**), indicating that the MAX crystal structure of the basal

planes is maintained in the MXene flake and is free of defects.[27, 28] The fast Fourier transform (FFT) of the TEM image (**Figure S3**) shows the hexagonal arrangement of atoms.[29] A high-resolution TEM (HR-TEM) image of MXene nanoflakes shows a lattice fringe spacing of 0.26 nm, corresponding to the (101) plane of MXene (**Figure 2e**).[2] **Figures 2f** and **2g** show the TEM, high-angle annular dark field scanning TEM (HAADF-STEM) and energy dispersive X-ray spectroscopy (EDS) elemental maps of the alkali-treated MXene/BC samples before annealing. The long BC nanofibers forms a sparse interwoven mesh that captures the 2D MXene flakes, demonstrating how the BC and MXene hybridize into a 1D/2D composite structure (**Figure 2f**). Titanium (Ti) is only found in the MXene nanoflakes; carbon (C) is distributed uniformly on the MXene/BC. The signal from Al is similar to the background counts in the EDS spectrum (**Figure S4**), indicating that the Al had been entirely removed from the MAX phase during HCl/LiF etching. **Figure 2h** and **2i** show the TEM image, HAADF-STEM and EDS maps of alkali-treated MXene/BC after annealing at 400 °C for 2 h in an Ar atmosphere. Under the protection of the Ar atmosphere, the morphologies of 2D MXene and 1D BC could still be well maintained even after annealing at 400 °C for 2 h.

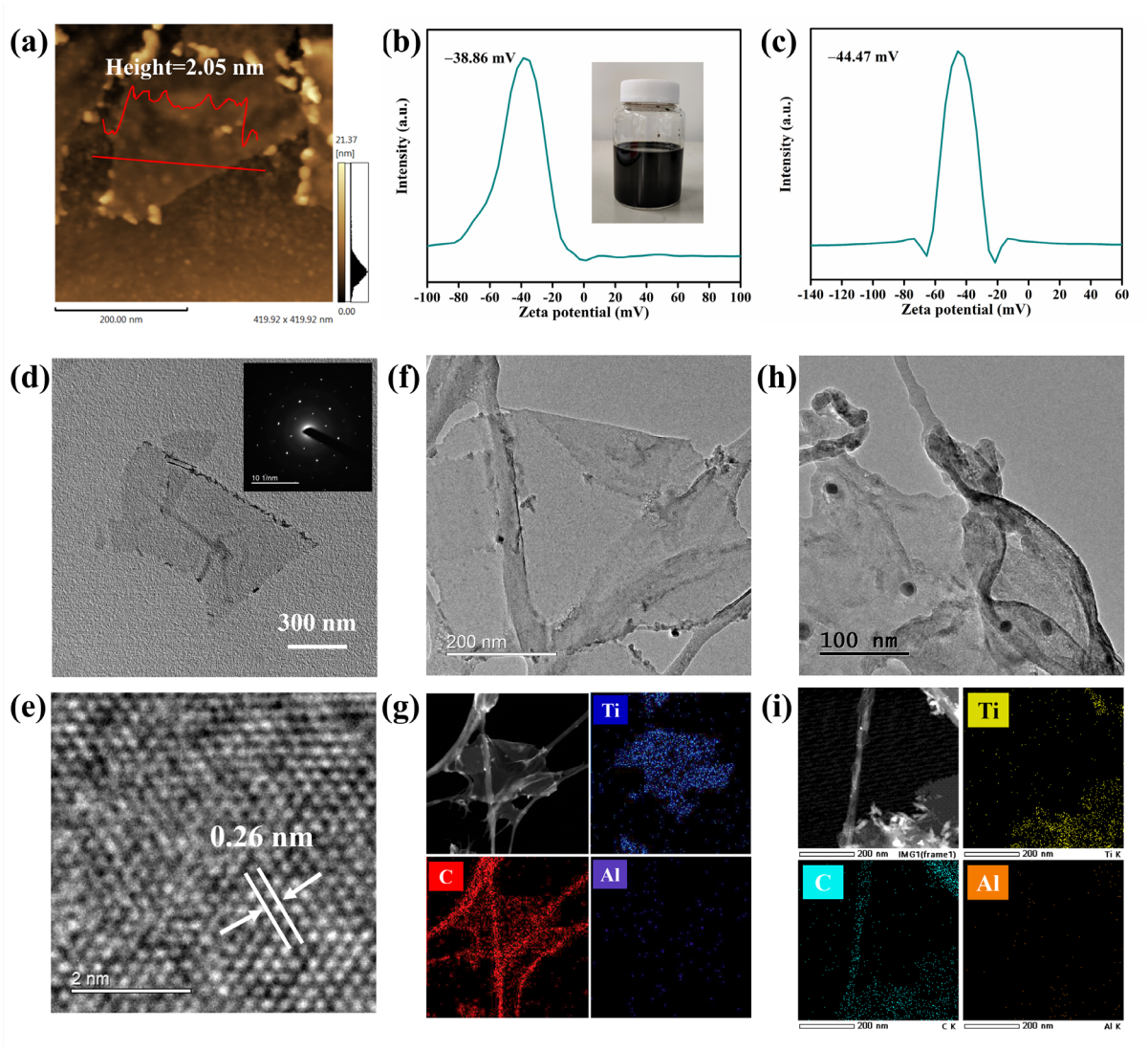

Figure 2. (a) AFM image of the MXene nanoflakes. Zeta potential distribution curves of (b) the MXene, and (c) BC suspensions. (d) TEM image and corresponding SAED pattern of MXene nanoflakes. (e) HR-TEM image of the MXene nanoflakes shows the (101) fringe spacing. (f) TEM image, and (g) HAADF-STEM-EDS elemental maps of alkali-treated MXene/BC before annealing. (h) TEM image, and (i) HAADF-STEM-EDS elemental maps of alkali-treated MXene/BC after annealing.

Due to the stability and effective cross-linking of the 1D BC nanofibers with 2D MXene nanoflakes in the colloidal mixture, a series of A-M/BC composite films were successfully fabricated. **Figure 3a** shows photographs and SEM images of the pure MXene, A-M/BC-0, A-M/BC-0.1, A-M/BC-0.2, and A-M/BC-0.5 films. The surface of the pure MXene film appears smooth and flat, while the surface of A-M/BC films after alkali treatment and

annealing tend to be rougher with the increase of BC content (top photographs of **Figure 3a**). Compared with the pure MXene film, some wrinkled nanoflakes and BC nanofibers can be observed from the top-view SEM images of the A-M/BC films (bottom SEM images of **Figure 3a, Figure S5**). However, as seen from the top-view SEM image of A-M/BC-0.5, the MXene nanoflakes and BC nanofibers are cross-linked with each other, and the broken MXene nanoflakes are apparent, destroying the surface integrity of the MXene film. Moreover, from the cross-sectional SEM image of A-M/BC-0.5 (**Figure S6**), the interlayer spacing of the A-M/BC-0.5 seems to be too large, which indicates a significant microstructure change of the MXene film caused by the addition of excessive BC. The morphological properties of the pure BC and M/BC films were also investigated, with photographs and top-view SEM images shown in **Figure S**7. The pure BC film is sufficiently transparent to transmit images and text(**Figure S**7**a**), while the M/BC film is smooth and opaque (**Figure S**7**b**). It can be seen from the SEM images that the surface of BC film is composed of nanofibers without channels or wrinkles, while 3D channels or wrinkles can be seen on the surface of the M/BC film (**Figure S**7**c, d**).

In order to explore the interlayer structure of the films, the cross-sectional SEM images of the BC, pure MXene, A-M/BC-0, and A-M/BC-0.2 films were obtained (**Figure S**8). 1D nanofibers with large aspect ratios can be observed in the cross-sectional SEM image of the BC film (**Figure S**8**a**), but the BC nanofibers are challenging to observe in the alkali-treated MXene/BC composite films due to a low concentration of BC (**Figure S**8**d**). The cross-sectional SEM image of the pure MXene film shows a tightly packed lamellar structure (**Figure S**8**b**), and the cross-sectional SEM images of the A-M/BC-0 film (**Figure S**8**c**) and A-M/BC-0.2 film (**Figure S**8**d**) reveal that MXene-based film still maintains a lamellar structure after alkali and annealing treatments. Furthermore, the cross-sectional views indicate that the A-M/BC-0.2 film has a more loose and porous interlayer space than A-M/BC-0 and pure MXene film, and the thickness of all the as-prepared MXene-based films are in the range

of 3−4 μm. The expansion of interlayer space and the increase of pores will be examined in detail later.

The corresponding EDS maps of Al, Ti, C, O, Na, Cl, and F were collected on the SEM cross-sections to compare the elemental distributions of pure MXene (**Figure 3b, Figure S9**) and A-M/BC-0.2 (**Figure 3c, Figure S10**) films. Both Ti and C are homogenously distributed, while Al is mostly removed except in a few locations. The pure MXene film contain O, F and Cl due to the etching step, but no Na is present in principle (**Figure S9**). The A-M/BC-0.2 film prepared by surface group regulation contains O, F, Cl and Na elements, but the concentration of both F and Cl is markedly reduced, while O concentration is higher due to the partial oxidation of the MXene after the alkali and annealing treatments (**Figure S10**).

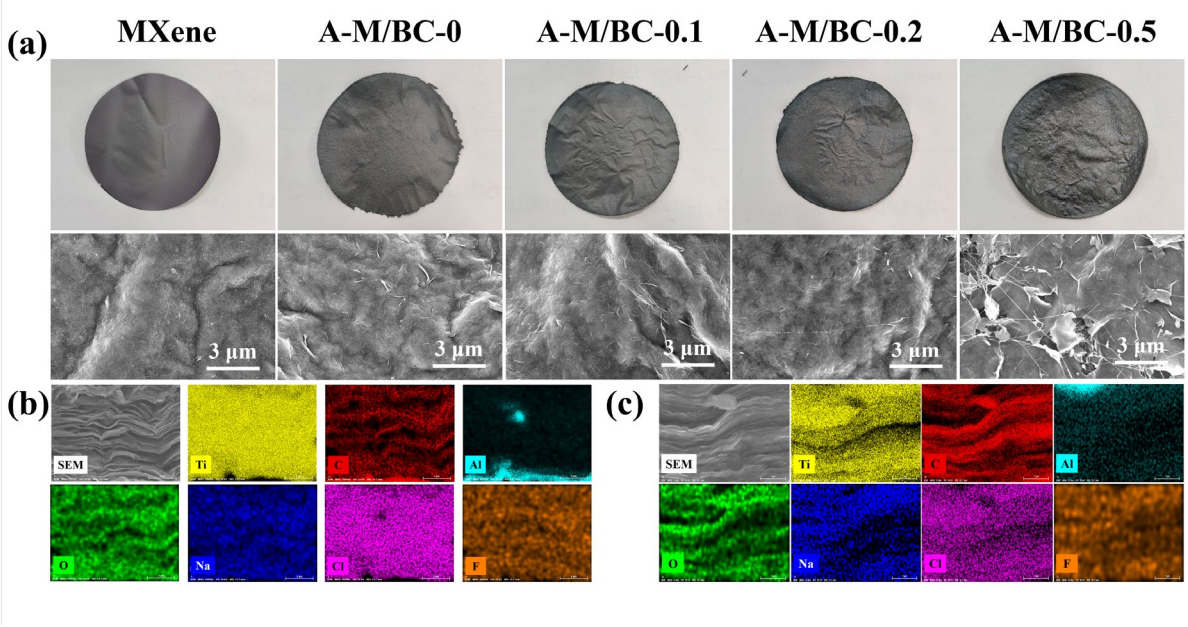

Figure 3. (a) Photographs (top) and SEM images (bottom) of the film electrodes. SEM-EDS maps of (b) the pure MXene film, and (c) the A-M/BC-0.2 film.

The crystalline properties of the as-prepared samples were confirmed using X-ray diffraction (XRD). **Figure 4a** shows the XRD patterns of Ti_3AlC_2 powder, pure MXene ($Ti_3C_2T_x$) film, and M/BC film, the enlarged patterns on the right show the (002) lattice plane. The results show that the characteristic peaks of Ti_3AlC_2 (JCPDS No. 52-0875) are substantially different from the patterns of both the MXene film and M/BC film, indicating

significant crystal structure modification. The (002) peak shifts to the left as the Al is removed from the MAX phase.[30] The XRD pattern of the pure BC film is shown in **Figure S11**. Since the added amount of the BC is too small to show the diffraction peak of BC in the XRD pattern of the M/BC film, the effect of its addition on the MXene can be evaluated by the shift of the (002) peak. As shown in **Figure 4a**, the (002) peak shifts from 6.9° ($d_{(002)}$ = 12.78 Å) for the pure MXene film to 6.8° ($d_{(002)}$ = 12.99 Å) for the composite M/BC film, corresponding to an increase in spacing of ~0.21 Å which is attributed to BC behaving like a 1D pillar to expand the interlayer space between the MXene nanoflakes.

The XRD patterns of the pure MXene, A-M/BC-0, A-M/BC-0.1, A-M/BC-0.2 and A-M/BC-0.5 films are shown in **Figure 4b**. Annealing the MXene films at 400 °C under Ar atmosphere results in no noticeable changes in the short-range crystal structure. The $d_{(002)}$ of the pure MXene, A-M/BC-0, A-M/BC-0.1, A-M/BC-0.2 and A-M/BC-0.5 films are 12.83 Å, 13.06 Å, 13.18 Å, 13.42 Å and 13.55 Å, respectively. The variation of the $d_{(002)}$ calculated by XRD patterns appears to be qualitatively consistent with the cross-sectional SEM images, and the $d_{(002)}$ expands with increasing amounts of BC. BC nanofibers mitigate the re-stacking of the MXene nanoflakes and expand the interlayer space of 3D channels between the MXene nanoflakes. Such a morphology is attractive because larger interlayer porosity can accelerate the diffusion of electrolyte ions, impacting the specific capacitance and rate performance of the film electrodes.[31, 32]

Figure 4c shows the Raman spectra of the pure MXene, A-M/BC-0, A-M/BC-0.1, A-M/BC-0.2 and A-M/BC-0.5 films. For clarity, the enlarged Raman spectrum of the pure MXene film is also provided in **Figure S12**. Raman peaks (**Figure 4c, S12**) in the range of 150-800 cm^{-1} correspond to the in-plane (E_g peaks, 290, 385, and 632 cm^{-1}) and out-of-plane (A_{1g} peaks, 201, 583, and 724 cm^{-1}) vibrations of Ti and C atoms as well as the functional groups in $Ti_3C_2T_x$ MXene.[33, 34] The characteristic peaks of A-M/BC-0, A-M/BC-0.1, A-

M/BC-0.2 and A-M/BC-0.5 films do not significantly change either in position or in intensity, indicating that MXene can maintain its stability even after the surface groups regulation process. Meanwhile, subjugating MXene-based films to the annealing step generated two prominent peaks at 1377 and 1586 cm^{-1}, corresponding to the D and G peaks of graphitic carbon. The I_D/I_G values of the composite films decreased with increasing amounts of BC (I_D/I_G=0.76 for the A-M/BC-0, I_D/I_G=0.67 for the A-M/BC-0.5).

The effect of annealing on the surface functional groups of the MXene-based films can also be observed with Fourier transform infrared (FTIR) spectroscopy (**Figure 4d**)**.** Pure MXene has peaks at 1738 cm^{-1} and 1384 cm^{-1}, which match O−H stretching and bending vibrations. Peaks at 1628 cm^{-1} and 1049 cm^{-1} match the C=O bond and C−F bonds, which confirm the expectation that the MXenes etched with HCl/LiF are coated with −OH, C=O, and C−F surface functional groups.[35] Interestingly, the FTIR spectra of the A-M/BC-0, A-M/BC-0.1, A-M/BC-0.2, and A-M/BC-0.5 films do not have peaks corresponding to O−H (~1738 cm^{-1}, ~1384 cm^{-1}) and C−F (~1049 cm^{-1}) bonds, indicating that alkali and annealing treatments remove these bonds. **Figure S13** shows the FTIR spectra of the A-M/BC-0.2 film collected three times, also showing the consistency of the observation that O−H and C−F are largely removed in the treatment process. The peaks at 1628 cm^{-1} and 522−565 cm^{-1} correspond to the C=O and Ti−O bonds, indicating that the MXene is unaffected by the 400 °C annealing step. The peak at 3428 cm^{-1} corresponds to the stretching vibration of the −OH group in MXene.[36, 37] Cellulose has known FTIR peaks at 3428 cm^{-1} and 1628 cm^{-1}, corresponding to O−H stretching and bending modes.[38] Also, increasing BC concentrations in the A-M/BC samples appear to cause a slight leftward shift in the Ti−O peak.

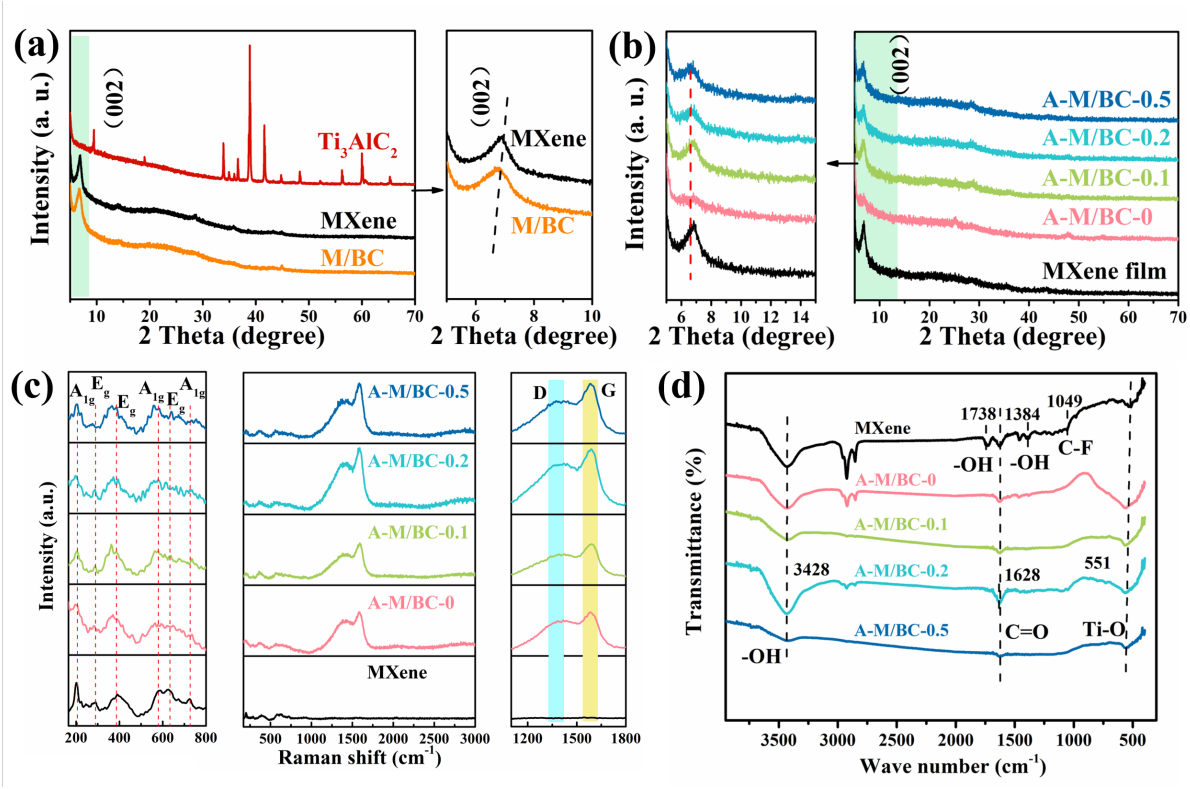

Figure 4. (a) XRD patterns of the Ti_3AlC_2 powder, pure $Ti_3C_2T_x$ MXene film, and M/BC film, and the enlarged patterns of the diffraction peaks at the (002) lattice plane. (b) XRD patterns of the pure MXene, A-M/BC-0, A-M/BC-0.1, A-M/BC-0.2, and A-M/BC-0.5 films. (c) Raman, and (d) FTIR spectra collected from the surfaces of the pure MXene, A-M/BC-0, A-M/BC-0.1, A-M/BC-0.2, and A-M/BC-0.5 film electrodes. The 200 to 800 cm^{-1} and 1150 to 1800 cm^{-1} sections of the Raman spectra were expanded to show the features of MXene and graphitic carbon more clearly.

Detailed analysis with X-ray photoelectron spectroscopy (XPS) is necessary to evaluate the impact of the alkali and annealing treatments on the surface structure and functional groups of the MXene/BC composites. Subtle changes in XPS binding energies can help us to elucidate changes in chemical state and environment that provide information on the presence of functional groups and local bonding environments. **Figure 5a** shows that the surfaces of the MXene, A-M/BC-0, A-M/BC-0.1, A-M/BC-0.2, and A-M/BC-0.5 films are primarily composed of Ti and C. Compared to the XPS survey spectrum of the MXene film, the F and

Cl peaks almost disappeared in the A-M/BC-0, A-M/BC-0.1, A-M/BC-0.2, and A-M/BC-0.5 films, while the Na KLL Auger peak appeared. The intensities of the O peaks increased, indicating that the alkali and annealing treatments eliminated a large amount of −F and −Cl functional groups and increased −O functional groups simultaneously. Some Na moiety is deposited on the surface of the MXene-BC composite films. Furthermore, with the increase of the BC content, the intensities of C peak for A-M/BC composite films are also increased. For clarity and brevity, A-M/BC-0.2 was selected for comparison with the pure MXene, the high-resolution XPS spectra for the Ti 2p C 1s, O 1s, F 1s, Cl 2p, and Na 1s peaks are shown in **Figure 5(b-g)** in detail. As shown in the **Figure 5b**, the high-resolution spectrum of Ti 2p for the A-M/BC-0.2 film have four doublets that match binding energies characteristic of Ti−C $2p_{3/2}$ (455.4 eV), Ti−O−C $2p_{3/2}$ (456.3 eV), C−Ti−F $2p_{3/2}$ (457.6 eV), Ti−O $2p_{3/2}$ (459.1 eV), Ti−C $2p_{1/2}$ (461.1 eV), Ti−O−C $2p_{1/2}$ (462.0 eV), C−Ti−F $2p_{1/2}$ (463.3 eV) and Ti−O $2p_{1/2}$ (464.8 eV) bonds.[39] Compared with the MXene film, the peak intensity of the C−Ti−F bond is weaker, and the Ti−O bonds are stronger in the XPS spectrum of the A-M/BC-0.2 film, indicating that the treatment steps increase the concentration of TiO_2 on the surface, while the concentration of the F element decreases. The decrease in the Ti 2p peak in the A-M/BC-0.2 film is due to the BC composite. The high-resolution spectra of the C 1s (**Figure 5c**) for the A-M/BC-0.2 film have five characteristic peaks representing the C−Ti (281.9 eV), C−Ti−O (282.3 eV), C−C (284.8 eV), C−O (286.1 eV), and O−C=O (289.2 eV) bonds.[40, 41] After the incorporation and partial carbonization of the BC, the intensities of the C−C and O−C=O bonds in the A-M/BC-0.2 film are more prominent than in the MXene film. Meanwhile, the incorporation of BC between the MXene weakens the C−Ti and C−Ti−O bonds. The high-resolution spectra of the O 1s (**Figure 5d**) also has five peaks matching the binding energies associated with the Ti−O, C−Ti−O, C−Ti−(OH), C=O, and H−O bonds.[37] The alkali and annealing treatments increased the oxygen concentration in the A-M/BC films. The relative change in concentration between the pure MXene and the MXene/BC composite films was

estimated by comparing the F 1s and Cl 2p peaks (**Figure 5e, f**). The 685.3 eV peak in the F 1s spectrum match C−Ti−F, while the two peaks at 199.4 eV and 201.0 eV in the Cl 2p spectrum matched C−Ti−Cl $2p_{3/2}$ and C−Ti−Cl $2p_{1/2}$, respectively. These results indicate that the F and Cl content significantly decreased in the A-M/BC-0.2 film relative to the pure MXene film. **Figure 5g** shows the characteristic peaks at 1072.1 and 1068.9 eV of the electronic environment of the C−Ti−Na bond and Ti LMM Auger peak, which implies that the surface of the A-M/BC-0.2 film contains an Na moiety.

The combined observations from XPS, SEM-EDS and FTIR discussed above demonstrate that the alkali and annealing treatment steps effectively modulate the surface functional groups of the composite MXene films. The two steps effectively replace or eliminate −F, −Cl, and −OH groups from the surface, leaving mainly −Na, −O functional groups. Such a significant change in the surface groups should have a measurable impact on the electrochemical properties of these composite film electrodes (**Figure 5h**). Furthermore, N_2 adsorption/desorption measurements were carried out at 77 K to compare the specific surface areas and pore size distributions of the pure MXene and the A-M/BC-0.2 films (**Figure 5i, j**). As mentioned before, the specific surface areas of the MXene and A-M/BC-0.2 films are 33.09 and 62.47 $m^2\ g^{-1}$, respectively, according to N_2 adsorption/desorption analysis. From this data, the BJH pore size distribution is used to estimate the average pore size of the films. The average pore size of the A-M/BC-0.2 film is 3.82 nm while the pure MXene film is 2.18 nm (**Figure 5j**). As a result, the methods used in the present work increased the specific surface area by ~2X and the pore size by ~50%. The 1D BC acts as pillar supports among the layers of MXene to hinder restacking of the 2D nanoflakes. Combining alkali and annealing treatments enables the composite film to retain more exposed active sites and helps create larger pore channels, which should promote ion transport and enhance the overall electrochemical performance of the composite film electrodes. Furthermore, the obtained

binder-free flexible A-M/BC-0.2 film shows good flexibility, it can be bent multiple times without any damage, as shown in **Figure S14a**. To verify the stability of the film electrode for practical applications, the flexible A-M/BC-0.2 film electrode was soaked in the 3M H_2SO_4 electrolyte. After three days of soaking, the film electrode can still maintain good flexibility after drying (**Figure S14b**).

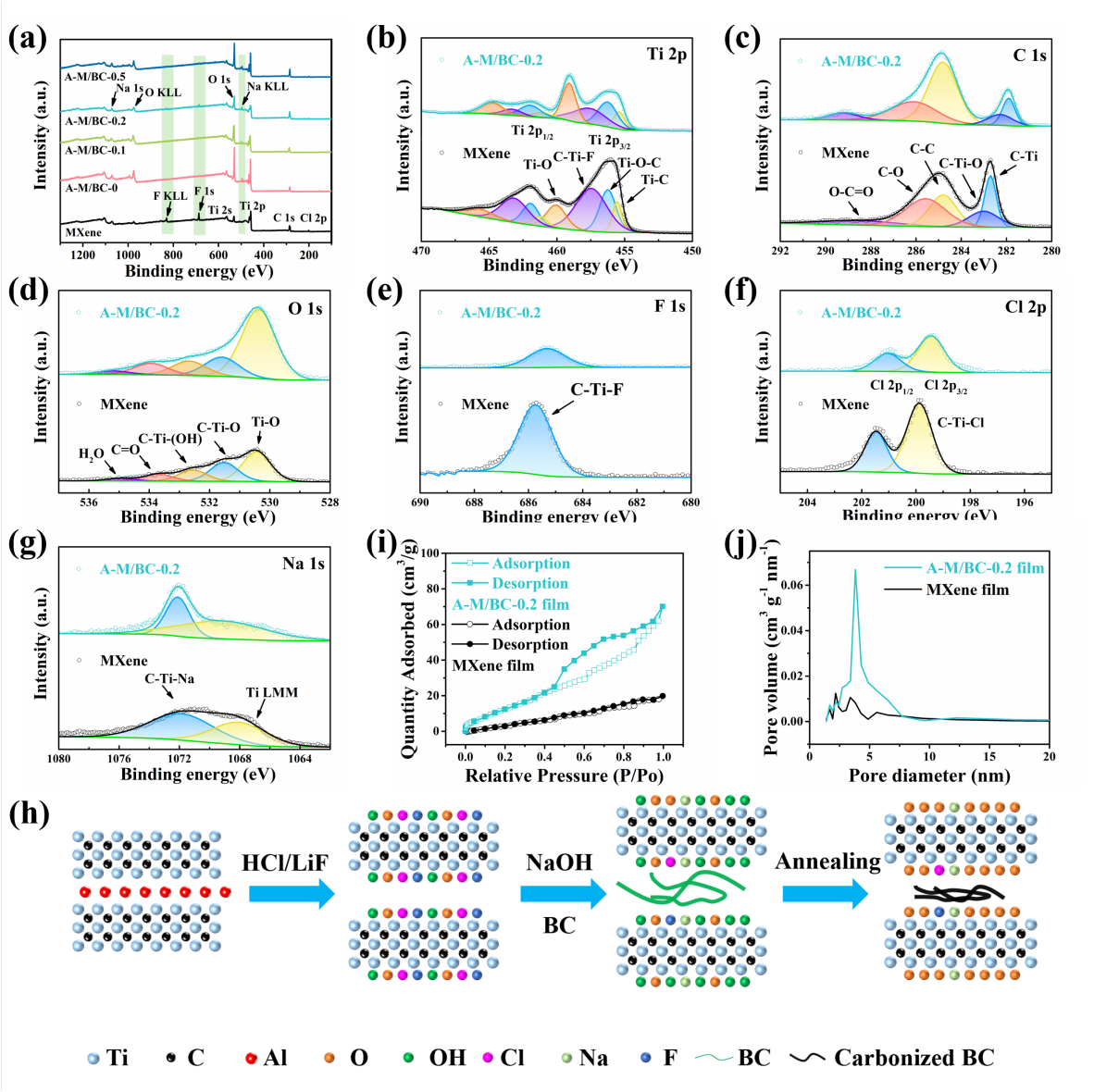

Figure 5. (a) XPS survey spectra of the pure MXene, A-M/BC-0, A-M/BC-0.1, A-M/BC-0.2, and A-M/BC-0.5 films. High-resolution XPS spectra for the Ti 2p (b), C 1s (c), O 1s (d), F 1s (e), Cl 2p (f), and Na 1s (g) peaks of the pure MXene and A-M/BC-0.2 films. (h) A scheme showing the etching of the MAX phase and modulation of the functional groups by forming

the MXene-BC composite with NaOH treatment and then the annealing treatment at 400 °C to form the A-M/BC film. (i) N_2 adsorption/desorption isotherms show that the A-M/BC-0.2 film has ~2X larger specific surface area than the pure MXene film. (j) BJH pore size distribution of the pure MXene and A-M/BC-0.2 films.

The electrochemical performance of the film electrodes was evaluated using a typical Swagelok three-electrode configuration in the potential range of −1.1 to −0.1 V (vs. Hg/Hg_2SO_4) in an aqueous 3M H_2SO_4 electrolyte solution with over-capacitive activated carbon as the counter electrode (**Figure 6a**). We initially compared the electrochemical properties of the pure MXene film versus an M/BC film electrode that had not been alkali-treated or annealed. The M/BC and pure MXene film electrodes have similar cyclic voltammetry (CV) and galvanostatic charge/discharge (GCD) curves, indicating they are pseudocapacitive in the H_2SO_4 electrolyte.[42] The integral area of the CV curves and discharge time in the GCD curves are notably smaller for the M/BC electrode versus pure MXene (**Figure S15, S16**). Correspondingly, the calculated specific capacitance of the M/BC film is 237 F g^{-1} at a current density of 1 A g^{-1}; and 220 F g^{-1} at a scan rate of 2 mV s^{-1}. The calculated specific capacitance of pure MXene is 298 F g^{-1} at a current density of 1 A g^{-1}; and 285 F g^{-1} at a scan rate of 2 mV s^{-1}. The reduced specific capacitance of the M/BC film is likely due to the insulating properties of BC.[11] Therefore, the direct addition of BC without alkali or annealing treatment does not enhance the electrochemical performance of the MXene-based composite films.

Figure 6b-f show the electrochemical properties of the pure MXene, A-M/BC-0, A-M/BC-0.1, A-M/BC-0.2, and A-M/BC-0.5 film electrodes. **Figure 6b** displays the CV curves at a scan rate of 20 mV s^{-1}. The integral area of the A-M/BC-0.2 film electrode is much larger than that of pure MXene, A-M/BC-0, A-M/BC-0.1, and A-M/BC-0.5 film electrodes. According to GCD curves at 1 A g^{-1}, the discharge time of the A-M/BC-0.2 film electrode is

also longer than the other film electrodes (**Figure 6c**). Furthermore, the rate performance of the A-M/BC-0.2 sample is 79% from 1 A g^{-1} to 50 A g^{-1}, which indicates an excellent coulombic efficiency at different current densities (**Figure 6d**). In addition, the CV curves of the A-M/BC-0.2 film electrode exhibit a pair of broad redox peaks, which retain their shape as the scan rate increases from 2 to 200 mV s^{-1} (**Figure 6e**). The GCD curves of the A-M/BC-0.2 film electrode also exhibit a highly symmetrical shape and have a slight charge/discharge plateau while the current density increases from 1 to 50 A g^{-1} (**Figure 6f**). The above results demonstrate that the A-M/BC-0.2 electrode has a superior rate capability and pseudocapacitive behavior.[43] As a result, the A-M/BC-0.2 film electrode delivers a gravimetric capacitance of 594 F g^{-1}, an areal capacitance of 874 mF cm^{-2}, and a volumetric capacitance of 2186 F cm^{-3} at a current density of 1 A g^{-1}, which is much higher than the other film electrodes we tested. **Table 1** displays the combined areal capacitance (C*s*, mF cm^{-2}), volumetric capacitance (C*v*, F cm^{-3}) and gravimetric capacitance (C*g*, F g^{-1}) of the film electrodes. Interestingly, the A-M/BC-0.2 film electrode capacitance is 2X larger than the pure MXene (298 F g^{-1}) and A-M/BC-0 (309 F g^{-1}) film electrodes. It is also notable that the gravimetric capacitance of the A-M/BC-0.2 film electrode is higher than most MXene-based materials reported in the literature (*i.e.*, **Table S2**: S, N-codoped MXene/rGO hybrid films (246.9 F g^{-1}, 1 A g^{-1}),[44] $Ti_3C_2T_x$ (490 F g^{-1}, 1 A g^{-1}),[45] 3D porous oxidation-resistant MXene/graphene (393 F g^{-1}, 2 mV s^{-1}),[46] Co-PC@MX-CNF (426.7 F g^{-1}, 1 A g^{-1}),[47] MXene/Graphdiyne nanotube (337.4 F g^{-1}, 2 A g^{-1}),[48] PANI/$Ti_3C_2T_x$ (462 F g^{-1}, 1 A g^{-1})[49]). NaOH and BC are both inexpensive, Earth-abundant reagents. Our method of treating MXenes with NaOH followed by low-temperature annealing is a simple method to improve the performance of these materials at a lower economic cost.

The CV and GCD measurements demonstrate that the specific capacitances of all A-M/BC film electrodes are higher than pure MXene film electrode. SEM-EDS, FTIR and XPS

measurements show that the NaOH replaces unfavorable −F groups to −OH and −Na groups, while the annealing step converts the −OH groups to −O groups. The removal of unfavorable groups (−OH, −F) and the increase of favorable −O groups contribute to the improvement of the conductivity and capacitance of MXene. Moreover, adding −Na groups help expand the interlayer space between MXene flakes. Meanwhile, the annealing at 400 ℃ results in partial carbonization of BC. Moderate carbonization can improve the conductivity of the MXene-based composite film, thereby improving its performance. However, excessive carbonization can negatively affect conductivity, which electrochemical impedance spectroscopy (EIS) analysis will describe in more detail.

Table 1. The gravimetric capacitance (C_g, F g^{-1}), areal capacitance (C_s, mF cm^{-2}) and volumetric capacitance (C_v, F cm^{-3}) of the film electrodes was calculated using GCD curves at a current density of 1 A g^{-1}.

sample	Pure MXene	A-M/BC-0	A-M/BC-0.1	A-M/BC-0.2	A-M/BC-0.5
C_g (F g^{-1})	298	309	356	594	337
C_s (mF cm^{-2})	427	468	524	874	497
C_v (F cm^{-3})	1255	1338	1380	2186	552

A previously reported method was used to analyze the capacitive contribution of the A-M/BC-0.2 film electrode at different scan rates.[50] The current response at a fixed potential is the combination of two separate mechanisms, surface capacitive and diffusion-controlled contribution processes:

$$i(V) = k_1 v + k_2 v^{1/2} \quad (1)$$

Equation (1) can be converted into:

$$i(V)/v^{1/2} = k_1 v^{1/2} + k_2 \quad (2)$$

where k_1 and k_2 are constants obtained from CV profiles at different scan rates. And $k_1 v$ and $k_2 v^{1/2}$ represent the current contributions from the surface capacitive and diffusion-controlled contributions, respectively.[51] The surface capacitive contribution increases from 84.7 % at a scan rate of 2 mV s^{-1} to 98.6 % at 200 mV s^{-1} (**Figure 6g**), implying there are reduced ion

diffusion pathways and rapid electron transfer, contributing to better rate capability and cycling stability as well as high current cycling capability.[52] EIS is an essential method for studying the electrochemical properties of the film electrodes. The Nyquist plots of the pure MXene, A-M/BC-0, A-M/BC-0.1, A-M/BC-0.2, A-M/BC-0.5, and M/BC film electrodes are shown in **Figure 6h**. The internal resistance (R_s) values are 4.15, 1.98, 1.64, 1.83, 2.77, and 6.97 Ω, respectively. Also, the fitted charge transfer resistance (R_{ct}) from the diameter of the semicircle is obtained according to the equivalent circuit described in the inset of **Figure 6h**. The R_{ct} of the pure MXene, A-M/BC-0, A-M/BC-0.1, A-M/BC-0.2, A-M/BC-0.5, and M/BC film electrodes after the fitting are 7.33, 0.51, 0.76, 0.99, 3.12, and 8.34 Ω, respectively. In addition, the time constant τ can be obtained by the equation of $\tau=1/f$ from the Bode plots of the phase angle versus frequency (**Figure S17**), where f is the characteristic frequency at a phase angle of −45°. The τ of the pure MXene, A-M/BC-0, A-M/BC-0.1, A-M/BC-0.2, A-M/BC-0.5, and M/BC film electrodes are 3.94, 0.79, 0.54, 0.87, 2.84, and 8.33 s, respectively. The shorter τ indicates a faster frequency response and higher ion transfer rate.[53] Generally, the Nyquist plots in the low-frequency region are almost parallel to the imaginary axis, indicating a close-to-ideal capacitive behavior of the film electrodes.[54] These Bode plots show that the phase angles at a frequency of 0.01 Hz of the pure MXene, A-M/BC-0, A-M/BC-0.1, A-M/BC-0.2, A-M/BC-0.5, and M/BC film electrodes are −84.5°, −87.8°, −87.0°, −86.5°, −86.7°, and −82.0°, respectively, which shows characteristic of ideal capacitive behavior (**Table 2**). The above data collectively shows that the direct mixing of MXene and BC without further treatment (i.e., the M/BC) increased resistance and reduced the ion transfer rate of the film electrode because BC is an insulator. The alkali and annealing treatments can eliminate or replace −F, −OH functional groups with more favorable −O, −Na groups on the surface of the MXene. Finally, for the series of samples of A-M/BC-0, A-M/BC-0.1, A-M/BC-0.2, and A-M/BC-0.5, the *Rs*, *Rct*, and τ of the film electrode decreased and then increased with the addition of the BC. This observation may be explained because a moderate

amount of BC carbonization increased the film conductivity, too much BC produced structural changes and off-gassing during carbonization, which destroyed the structure of the film electrode. Moreover, the cycling stability is one of the vital electrochemical properties of the MXene-based film electrodes for SCs. GCD cycling tests were performed for the A-M/BC-0.2 film electrode at a current density of 50 A g^{-1}, which shows excellent electrochemical cycling stability and advantages in coping with large current shock, retaining 88.92% of the initial specific capacitance after 5000 charge/discharge cycles and 83.46 % after 10,000 cycles. Meanwhile, the coulombic efficiency of 101.22 % can be maintained (**Figure 6i**). Selected cycles (1−5 cycles vs. 9996−10000 cycles), as shown in the **Figure S18**, are similar in magnitude and possess symmetrical charging and discharging curves, indicating a high reversibility and cycling stability.

Table 2. EIS spectra data of the film electrodes.

Sample	*Rs* (Ω)	*Rct* (Ω)	τ (s)	Bode phase angle (°)
Pure MXene	4.16	7.33	3.94	−84.5
A-M/BC-0	1.98	0.51	0.79	–87.8
A-M/BC-0.1	1.64	0.76	0.54	–87.0
A-M/BC-0.2	1.83	0.99	0.87	–86.5
A-M/BC-0.5	2.77	3.12	2.84	–86.7
M/BC	6.97	8.34	8.33	–82.0

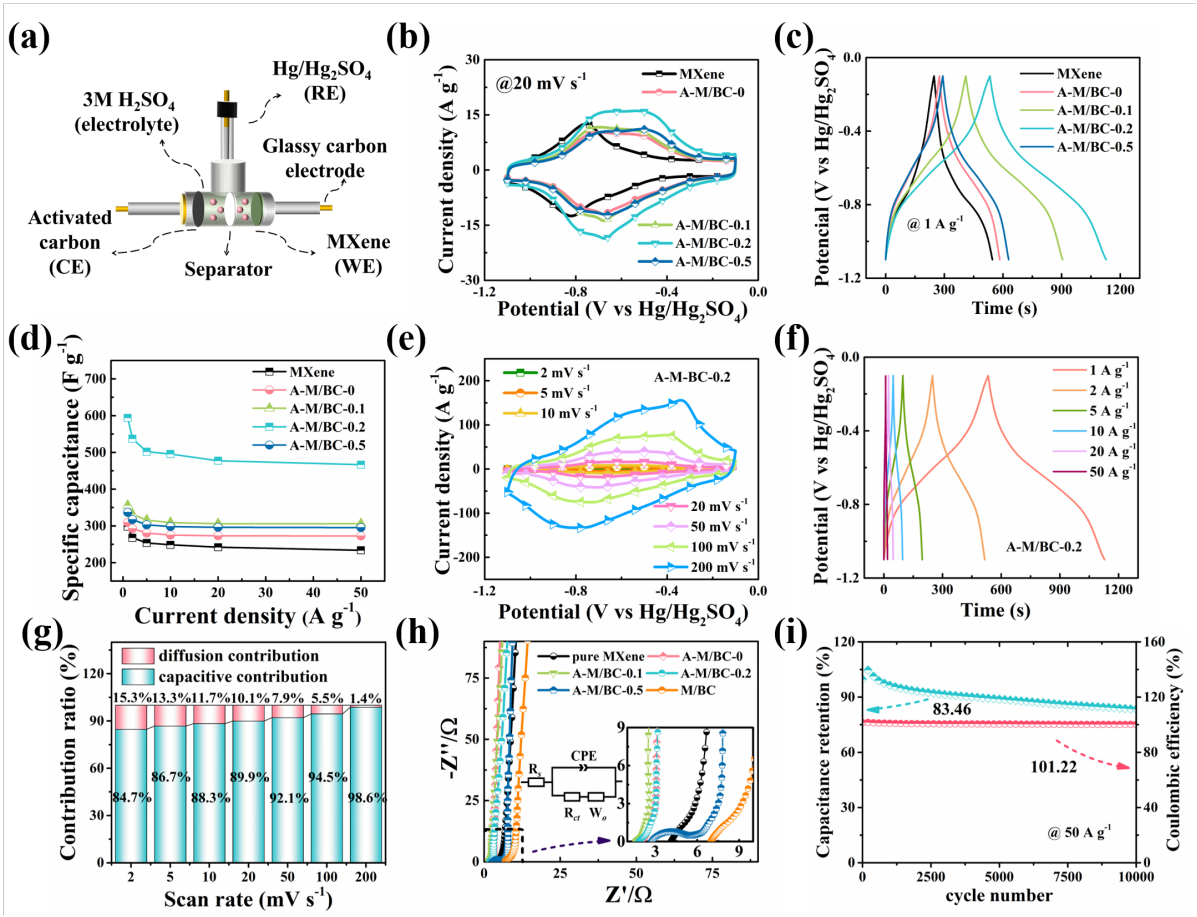

Figure 6. Electrochemical performance of the pure MXene, A-M/BC-0, A-M/BC-0.1, A-M/BC-0.2, and A-M/BC-0.5 composite film electrodes. (a) An illustration of the Swagelok three-electrode setup for evaluating the electrochemical performance of the MXene-based film electrodes. (b) CV curves at a scan rate of 20 mV s^{-1}. (c) GCD curves at a current density of 1 A g^{-1}. (d) Specific gravimetric capacitances are calculated from the GCD curves. (e) CV and (f) GCD curves of A-M/BC-0.2 film electrode at different scan rates and current densities. (g) Diffusion- and capacitive-controlled contributions of the A-M/BC-0.2 film electrode in CV test at different scan rates. (h) Nyquist plots of the film electrodes. A zoom-in image of the high freqency data is inset in the figure. (i) Capacitance retention and coulombic efficiency of the A-M/BC-0.2 film electrode during 10000 charge/discharge cycles (@ 50 A g^{-1}).

Two pieces of the A-M/BC-0.2 film were used to fabricate symmetric SCs (SSCs) and test the electrochemical performance at 0 to 1 V voltage range in a 3M H_2SO_4 electrolyte.

Figure 7a, b shows the CV and GCD curves of the SSC based on the A-M/BC-0.2 film are symmetrical in shape at scan rates from 1 to 100 mV s^{-1}, with current densities in the range of 0.5 to 10 A g^{-1}, demonstrating excellent electrochemical performance with high reversibility. As seen in **Figure 7c**, the specific gravimetric capacitance of the SSC is 277.23 F g^{-1} at a current density of 0.5 A g^{-1} and decays to 237.08 F g^{-1} at a current density of 10 A g^{-1}, resulting in a rate capability of 85.51 %. The inset of **Figure 7c** is the Nyquist plot of the SSC; the equivalent series resistance of the SSC is ~5.6 Ω, which further confirms the low resistance of the two-electrode system due to the good electrical conductivity of the active film electrode.

In addition, the energy density and power density of the device were calculated and plotted in a Ragone plot (**Figure 7d and Figure S19**). The A-M/BC-0.2-based SSC shows a maximum areal energy density of 13.38 μWh cm^{-2} at a power density of 347.37 μW cm^{-2}, and retains the areal energy density of 11.44 μWh cm^{-2} when the power density increases to 7537.13 μW cm^{-2} (**Figure S19**). The A-M/BC-0.2 based SSC has a the gravimetric energy density of 9.63 Wh kg^{-1} at a power density of 250 W kg^{-1}, which is comparable to or higher than other MXene-based SCs, such as the MXene/rGO (10.5 Wh kg^{-1} at 80.3 W kg^{-1}),[55] $MnO_2/Ti_3C_2T_x$ hybrid film (8.3 Wh kg^{-1} at 221.33 W kg^{-1})[56] and MXene//MnO_2 (6.4 Wh kg^{-1} at 1107.7 W kg^{-1}),[57] MXene/CNTs (2.77 Wh kg^{-1} at 311 W kg^{-1}),[58] Porous $Ti_3C_2T_x$/CNTs film (9.2 Wh kg^{-1} at 96.1 W kg^{-1}),[59] $Ti_3C_2T_x/Nb_2CT_x$ (5.7 Wh kg^{-1} at 172.5 W kg^{-1}),[60] 300-K-Ag-Ti_3CNT_x (7.3 Wh kg^{-1} at 350 W kg^{-1}),[61] N-$Ti_3C_2T_x$ (9.57 Wh kg^{-1} at 250 W kg^{-1}).[62] Furthermore, the energy density could be maintained at 8.23 Wh kg^{-1} even when the power density reaches 5424.45 W kg^{-1} (**Figure 7d**). Therefore, the films based on the A-M/BC-0.2 composite architecture are promising candidates for high-energy SSCs.

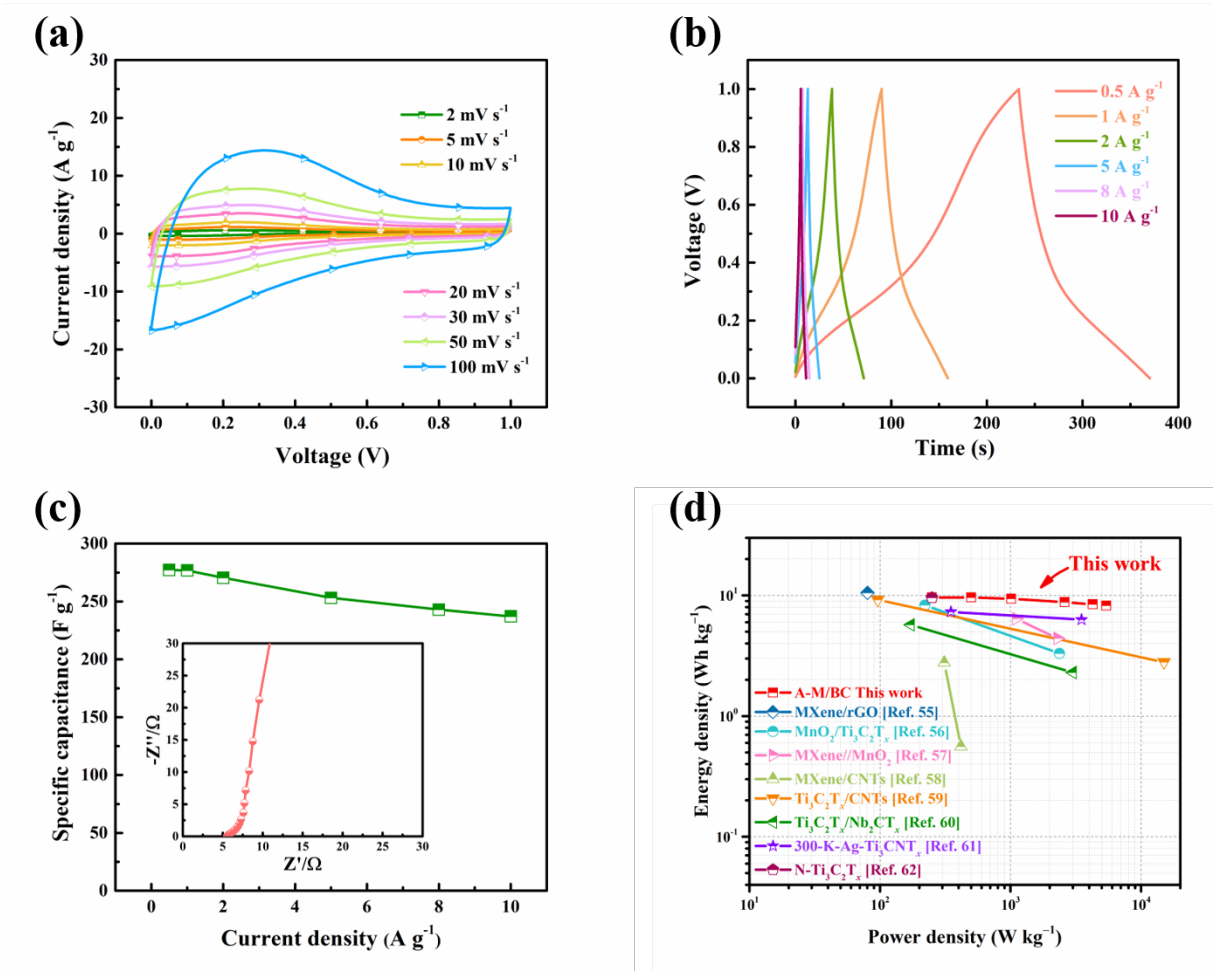

Figure 7. The electrochemical performance of an SSC based on the A-M/BC-0.2 film. (a) CV curves at various scan rates. (b) GCD curves at various current densities. (c) Specific gravimetric capacitances calculated from the GCD curves (the Nyquist plot of the SSC is inset in the figure). (d) Ragone plot comparing our composite MXene/BC electrode device with other MXene-based devices.

CONCLUSIONS

In this study, we introduced a straightforward and cost-effective technique using 1D BC, NaOH alkali treatment and low-temperature annealing to regulate the surface functional groups of the MXene/BC composite films and expand the interlayer space between 2D MXene nanoflakes. The BC prevents the MXene nanoflakes from re-stacking, enabling them to retain a large interlayer space containing numerous 3D micropores, resulting in a 2X larger specific surface area for the composite film (62.47 m^2 g^{-1}) versus the pure film (33.09 m^2 g^{-1}).

Partial carbonization of the BC forms a nanofibrous matrix of graphitic carbon that serves as a conductive nanoscale interlayer to enhance ion transport in SSCs. The alkali and annealing treatments reduced the unfavorable −OH, −F, and −Cl surface functional groups of MXene, leaving −Na and −O functional groups to mainly occupy the surface of MXene nanoflakes. As a result, our best-performing sample, A-M/BC-0.2, has a capacitance of 594 F g^{-1} at a current density of 1 A g^{-1} in 3M H_2SO_4 electrolyte, which is 2X larger than pure MXene (298 F g^{-1}) and the A-M/BC-0 (309 F g^{-1}). The corresponding film has an areal capacitance of 874 mF cm^{-2} and a volumetric capacitance of 2186 F cm^{-3} at a current density of 1 A g^{-1}, respectively. Furthermore, the capacitance retention of the film is 83.46 % capacitance retention after 10,000 charge/discharge cycles at 50 A g^{-1}. The corresponding SSC has an energy density of 9.63 Wh kg^{-1} at a power density of 250 W kg^{-1}. However, excessive BC incorporation and/or carbonization decreases the overall electrochemical performance of devices because too much BC during annealing destroys the microstructure of the MXene. This work offers an easy and inexpensive method to fabricate high-performance film electrodes for electronic devices and exemplifies the significance of regulating functional groups in MXenes for energy storage.

EXPERIMENTAL SECTION

Preparation of $Ti_3C_2T_x$ (MXene) nanoflakes

The Ti_3AlC_2 MAX powder was prepared by sintering a mixture of Ti, TiC, and Al in a molar ratio of 1:2:1.2 at 1350 ℃ for 2 h in a tube furnace under flowing Ar. The resulting solid was thoroughly pulverized and passed through a 400-mesh to produce the MAX powder. The obtained powder was then selectively etched with HCl and LiF to remove the Al atomic layer, resulting in $Ti_3C_2T_x$ MXene with a 2D structure, as described in our previous reports.[4] Specifically, 2 g LiF powder was dissolved in 20 mL of 9M HCl solution to obtain the etchant mixture. Then 1 g of Ti_3AlC_2 powder was slowly dispersed into the above solution while stirring vigorously at 35 °C for 24 h. After that, the collected sediment was centrifuged with ultrapure (UP) water at 3500 rpm for 5 min each time until the pH of the supernatant became

neutral. Next, the washed sediment was dispersed into 200 mL of UP water and sonicated in an ice bath for 2 h with Ar gas bubbling in the mixture. Finally, the sonicated solution was centrifuged at 3500 rpm for 45 min, and the supernatant with dark green color was collected for experiments. The concentration of $Ti_3C_2T_x$ MXene obtained was determined to be 0.5 mg mL^{-1}.

Preparation of Alkali-treated MXene/Bacterial Cellulose film

Alkali-treated MXene/Bacterial Cellulose (A-M/BC) films with different mass fractions of 1D BC fibers were prepared using a simple vacuum-assisted filtration method combined with low-temperature annealing. Firstly, the BC dispersions of 1 mg mL^{-1} were controllably added to the MXene colloid (15 mg, 0.5 mg mL^{-1}) solution above and stirred continuously for 20 min. Next, 150 mg mL^{-1} of NaOH solution was added to the BC and MXene mixture solution and stirred continuously for 60 min, where the mass ratio of NaOH: MXene: BC was maintained at 10:1:(0-0.5). Then, the flexible precursor films were prepared by vacuum-assisted filtration on a cellulose filter film (diameter: 50 mm; pore size: 0.22 μm), which were finally freeze-dried in a vacuum system overnight at −50 ℃ and peeled off from the filter paper. Finally, the flexible porous A-M/BC films were annealed in Ar at 400 ℃ for 2 h using a ramp rate of 3 ℃ min^{-1}.

ASSOCIATED CONTENT

Supporting Information

< Discussions of experimental details including chemicals, characterizations, electrochemical measurements, and calculation, SEM image of Ti_3AlC_2 powder, photograph of the $Ti_3C_2T_x$ colloidal suspension, a FFT taken from a TEM image of the MXene nanoflakes, EDS spectrum of the alkali-treated MXene/BC solution, photographs and SEMs of the film samples, SEM-EDS spectra and corresponding quantification report of the MXene film and the A-M/BC-0.2, XRD pattern of the pure BC film, Raman spectrum of the MXene film,

FTIR spectra of the A-M/BC-0.2 film collected three times, photographs of the mechanical flexibility test, electrochemical characterization of films, a table of the physical parameters of the films, and a table comparing MXene-based electrodes for supercapacitors>

Notes

The authors declare no competing financial interest.

ACKNOWLEDGMENTS

This work was supported by the Key Science and Technology Developing Project of Shaanxi Province (2020KWZ-004), the China Scholarship Council (CSC), the National Natural Science Foundation of China (52302366), the Natural Science Research Project of Shaanxi Province Education Department (23JK0539), and the Key Projects of the Natural Science Foundation of Shandong Province (ZR2020KF001). This work was also supported by the Japan Society for the Promotion of Science (JSPS) Grants-in-Aid for Scientific Research Kakenhi Program (20K05453) and the JST-ERATO Yamauchi Materials Space Tectonics Project (JPMJER2003). This work used the Queensland node of the NCRIS-enabled Australian National Fabrication Facility (ANFF).

REFERENCES

(1) Naguib, M.; Mochalin, V. N.; Barsoum, M. W.; Gogotsi, Y. 25th Anniversary Article: MXenes: A New Family of Two-Dimensional Materials. *Adv. Mater.* **2014**, *26*, 992-1005.

(2) Tang, J.; Mathis, T.; Zhong, X.; Xiao, X.; Wang, H.; Anayee, M.; Pan, F.; Xu, B.; Gogotsi, Y. Optimizing Ion Pathway in Titanium Carbide MXene for Practical High-Rate Supercapacitor. *Adv. Energy Mater.* **2021**, *11*, 2003025.

(3) Mohammadi, A. V.; Rosen, J.; Gogotsi, Y. The World of Two-Dimensional Carbides and Nitrides (MXenes). *Science* **2021**, *372*, 1165.

(4) Luo, Y.; Tang, Y.; Bin, X.; Xia, C.; Que, W. 3D Porous Compact 1D/2D Fe_2O_3/MXene Composite Aerogel Film Electrodes for All-Solid-State Supercapacitors. *Small* **2022**, *18*, 2204917.

(5) Luo, J.; Matios, E.; Wang, H.; Tao, X.; Li, W. Interfacial Structure Design of MXene-Based Nanomaterials for Electrochemical Energy Storage and Conversion. *InfoMat* **2020**, *2*, 1057-1076.

(6) Luo, J.; Zheng, J.; Nai, J.; Jin, C.; Yuan, H.; Sheng, O.; Liu, Y.; Fang, R.; Zhang, W.; Huang, H.; Gan, Y.; Xia, Y.; Liang, C.; Zhang, J.; Li, W.; Tao, X. Atomic Sulfur Covalently Engineered Interlayers of Ti_3C_2 MXene for Ultra-Fast Sodium-Ion Storage by Enhanced Pseudocapacitance. *Adv. Funct. Mater.* **2019**, *29*, 1808107.

(7) Wan, Y.; Xiong, P.; Liu, J.; Feng, F.; Xun, X.; Gama, F. M.; Zhang, Q.; Yao, F.; Yang, Z.; Luo, H.; Xu, Y. Ultrathin, Strong, and Highly Flexible $Ti_3C_2T_x$ MXene/Bacterial Cellulose Composite Films for High-Performance Electromagnetic Interference Shielding. *ACS Nano* **2021**, *15*, 8439-8449.

(8) Zheng, W.; Yang, Y.; Fan, L.; Ye, D.; Xu, W.; Xu, J. Ultralight PPy@PVA/BC/MXene Composite Aerogels for High-Performance Supercapacitor Electrodes and Pressure Sensors. *Appl. Surf. Sci.* **2023**, *624*, 157138.

(9) Yuan, T.; Zhang, Z.; Liu, Q.; Liu, X.; Miao, Y. N.; Yao, C. MXene ($Ti_3C_2T_x$)/Cellulose Nanofiber/Polyaniline Film As a Highly Conductive and Flexible Electrode Material for Supercapacitors. *Carbohydr. Polym.* **2023**, *304*, 120519.

(10) Lyu, S.; Chang, H.; Zhang, L.; Wang, S.; Li, S.; Lu, Y.; Li, S. High Specific Surface Area MXene/SWCNT/Cellulose Nanofiber Aerogel Film As an Electrode for Flexible Supercapacitors. *Composites, Part B* **2023**, *264*, 110888.

(11) Zhou, B.; Li, Q.; Xu, P.; Feng, Y.; Ma, J.; Liu, C.; Shen, C. An Asymmetric Sandwich Structural Cellulose-Based Film with Self-Supported MXene and AgNW Layers for Flexible Electromagnetic Interference Shielding and Thermal Management. *Nanoscale* **2021**, *13*, 2378-2388.

(12) Song, Q.; Zhan, Z.; Chen, B.; Zhou, Z.; Lu, C. Biotemplate Synthesis of Polypyrrole@Bacterial Cellulose/MXene Nanocomposites with Synergistically Enhanced Electrochemical Performance. *Cellulose* **2020**, *27*, 7475-7488.

(13) Wang, Y.; Wang, X.; Li, X.; Bai, Y.; Xiao, H.; Liu, Y.; Liu, R.; Yuan, G. Engineering 3D Ion Transport Channels for Flexible MXene Films with Superior Capacitive Performance. *Adv. Funct. Mater.* **2019**, *29*, 1900326.

(14) Chen, J.; Chen, H.; Chen, M.; Zhou, W.; Tian, Q.; Wong, C.-P. Nacre-Inspired Surface-Engineered MXene/Nanocellulose Composite Film for High-Performance Supercapacitors and Zinc-Ion Capacitors. *Chem. Eng. J.* **2022**, *428*, 131380.

(15) Sun, W.; Shah, S. A.; Chen, Y.; Tan, Z.; Gao, H.; Habib, T.; Radovic, M.; Green, M. J. Electrochemical Etching of Ti_2AlC to Ti_2CT_x (MXene) in Low-Concentration Hydrochloric Acid Solution. *J. Mater. Chem. A* **2017**, *5*, 21663-21668.

(16) Lukatskaya, M. R.; Bak, S. M.; Yu, X.; Yang, X. Q.; Barsoum, M. W.; Gogotsi, Y. Probing the Mechanism of High Capacitance in 2D Titanium Carbide Using In Situ X-Ray Absorption Spectroscopy. *Adv. Energy Mater.* **2015**, *5*, 1500589.

(17) Luo, J.; Tao, X.; Zhang, J.; Xia, Y.; Huang, H.; Zhang, L.; Gan, Y.; Liang, C.; Zhang, W. Se^{4+} Ion Decorated Highly Conductive Ti_3C_2 MXene: Promising Lithium-Ion Anodes with Enhanced Volumetric Capacity and Cyclic Performance. *ACS Nano* **2016**, *10*, 2491-2499.
(18) Peng, Q.; Guo, J.; Zhang, Q.; Xiang, J.; Liu, B.; Zhou, A.; Liu, R.; Tian, Y. Unique Lead Adsorption Behavior of Activated Hydroxyl Group in Two-Dimensional Titanium Carbide. *J. Am. Chem. Soc.* **2014**, *136*, 4113-4116.
(19) Lian, P.; Dong, Y.; Wu, Z.; Zheng, S.; Wang, X.; Wang, S.; Sun, C.; Qin, J.; Shi, X.; Bao, X. Alkalized Ti_3C_2 MXene Nanoribbons with Expanded Interlayer Spacing for High-Capacity Sodium and Potassium Ion Batteries. *Nano Energy* **2017**, *40*, 1-8.
(20) Zahra, S. A.; Murshed, M. M.; Naeem, U.; Gesing, T. M.; Rizwan, S. Cation-Assisted Self-Assembled Pillared V_2CT_x MXene Electrodes for Efficient Energy Storage. *Chem. Eng. J.* **2023**, *474*, 145526.
(21) Luo, J.; Wang, C.; Wang, H.; Hu, X.; Matios, E.; Lu, X.; Zhang, W.; Tao, X.; Li, W. Pillared MXene with Ultralarge Interlayer Spacing As a Stable Matrix for High Performance Sodium Metal Anodes. *Adv. Funct. Mater.* **2019**, *29*, 1805946.
(22) Luo, J.; Lu, X.; Matios, E.; Wang, C.; Wang, H.; Zhang, Y.; Hu, X.; Li, W. Tunable MXene-Derived 1D/2D Hybrid Nanoarchitectures As a Stable Matrix for Dendrite-Free and Ultrahigh Capacity Sodium Metal Anode. *Nano Lett.* **2020**, *20*, 7700-7708.
(23) Shen, X.; Hai, R.; Wang, X.; Li, Y.; Wang, Y.; Yu, F.; Ma, J. Free-Standing 3D Alkalized $Ti_3C_2T_x$/$Ti_3C_2T_x$ Nanosheet Membrane Electrode for Highly Efficient and Stable Desalination in Hybrid Capacitive Deionization. *J. Mater. Chem. A* **2020**, *8*, 19309-19318.
(24) Zhao, D.; Zhao, R.; Dong, S.; Miao, X.; Zhang, Z.; Wang, C.; Yin, L. Alkali-Induced 3D Crinkled Porous Ti_3C_2 MXene Architectures Coupled with NiCoP Bimetallic Phosphide Nanoparticles As Anodes for High-Performance Sodium-Ion Batteries. *Energy Environ. Sci.* **2019**, *12*, 2422-2432.
(25) Li, K.; Zhang, P.; Soomro, R. A.; Xu, B. Alkali-Induced Porous MXene/Carbon Nanotube-Based Film Electrodes for Supercapacitors. *ACS Appl. Nano Mater.* **2022**, *5*, 4180-4186.
(26) Prathapan, R.; Thapa, R.; Garnier, G.; Tabor, R. F. Modulating the Zeta Potential of Cellulose Nanocrystals Using Salts and Surfactants. *Colloids Surf., A* **2016**, *509*, 11-18.
(27) Wang, D.; Zhang, D.; Li, P.; Yang, Z.; Mi, Q.; Yu, L. Electrospinning of Flexible Poly(vinyl alcohol)/MXene Nanofiber-Based Humidity Sensor Self-Powered by Monolayer Molybdenum Diselenide Piezoelectric Nanogenerator. *Nano-Micro Lett.* **2021**, *13*, 57.
(28) Naguib, M.; Mashtalir, O.; Carle, J.; Presser, V.; Lu, J.; Hultman, L.; Gogotsi, Y.; Barsoum, M. W. Two-Dimensional Transition Metal Carbides. *ACS Nano* **2012**, *6*, 1322-1331.
(29) Ahmed, B.; Anjum, D. H.; Gogotsi, Y.; Alshareef, H. N. Atomic Layer Deposition of SnO_2 on MXene for Li-Ion Battery Anodes. *Nano Energy* **2017**, *34*, 249-256.
(30) Ghidiu, M.; Lukatskaya, M. R.; Zhao, M.-Q.; Gogotsi, Y.; Barsoum, M. W. Conductive Two-Dimensional Titanium Carbide 'Clay' with High Volumetric Capacitance. *Nature* **2014**, *516*, 78-81.
(31) Yan, B.; Feng, L.; Zheng, J.; Zhang, Q.; Dong, Y.; Ding, Y.; Yang, W.; Han, J.; Jiang, S.; He, S. Nitrogen-Doped Carbon Layer on Cellulose Derived Free-Standing Carbon Paper for High-Rate Supercapacitors. *Appl. Surf. Sci.* **2023**, *608*, 155144.
(32) Al Haj, Y.; Mousavihashemi, S.; Robertson, D.; Borghei, M.; Pääkkönen, T.; Rojas, O. J.; Kontturi, E.; Kallio, T.; Vapaavuori, J. Biowaste-Derived Electrode and Electrolyte Materials for Flexible Supercapacitors. *Chem. Eng. J.* **2022**, *435*, 135058.
(33) Sarycheva, A.; Gogotsi, Y. Raman Spectroscopy Analysis of the Structure and Surface Chemistry of $Ti_3C_2T_x$ MXene. *Chem. Mater.* **2020**, *32*, 3480-3488.
(34) Wu, F.; Qiang, S.; Zhu, X; Jiao, W.; Liu, L.; Yu, J.; Liu, Y; Ding, B. Fibrous MXene Aerogels with Tunable Pore Structures for High-Efficiency Desalination of Contaminated Seawater. *Nano-Micro Lett.* **2023**, *15*, 71.

(35) Nagarajan, R. D.; Sundaramurthy, A.; Sundramoorthy, A. K. Synthesis and Characterization of MXene ($Ti_3C_2T_x$)/Iron Oxide Composite for Ultrasensitive Electrochemical Detection of Hydrogen Peroxide. *Chemosphere* **2022**, *286*, 131478.
(36) Zhang, D.; Yang, K.; Zhang, T.; Luo, M.; Li, M.; Li, Z.; Liu, C.; Ling, Y.; Chen, W.; Zhou, X. A Facile "Thick to Thin" Strategy for Integrating High Volumetric Energy Density and Excellent Flexibility into MXene/Wood Free-Standing Electrode for Supercapacitors. *Chem. Eng. J.* **2023**, *460*, 141733.
(37) Wang, H.; Wang, Y.; Chang, J.; Yang, J.; Dai, H.; Xia, Z.; Hui, Z.; Wang, R.; Huang, W.; Sun, G. Nacre-Inspired Strong MXene/Cellulose Fiber with Superior Supercapacitive Performance via Synergizing the Interfacial Bonding and Interlayer Spacing. *Nano Lett.* **2023**, *23*, 5663-5672.
(38) Ma, C.; Cao, W.; Zhang, W.; Ma, M; Sun, W.; Zhang, J.; Chen, F. Wearable, Ultrathin and Transparent Bacterial Celluloses/MXene Film with Janus Structure and Excellent Mechanical Property for Electromagnetic Interference Shielding. *Chem. Eng. J.* **2021**, *403*, 126438.
(39) Shen, L.; Zhao, W.; Wang, K.; Xu, J. GO-Ti_3C_2 Two-Dimensional Heterojunction Nanomaterial for Anticorrosion Enhancement of Epoxy Zinc-Rich Coatings. *J. Hazard. Mater.* **2021**, *417*, 126048.
(40) Yang, S.; Yao, J.; Hu, H.; Zeng, Y.; Huang, X.; Liu, T.; Bu, L.; Tian, K.; Lin, Y.; Li, X.; Jiang, S.; Zhou, S.; Li, W.; Bashir, T.; Choi, J-H.; Gao, L.; Zhao, J. Sonication-Induced Electrostatic Assembly of an $FeCO_3$@Ti_3C_2 Nanocomposite for Robust Lithium Storage. *J. Mater. Chem. A* **2020**, *8*, 23498-23510.
(41) Wang, B.; Zhang, W.; Lai, C.; Liu, Y.; Guo, H.; Zhang, D.; Guo, Z. Facile Design of Flexible, Strong, and Highly Conductive MXene‐Based Composite Films for Multifunctional Applications. *Small* **2023**, *52*, 2302335.
(42) Lukatskaya, M. R.; Kota, S.; Lin, Z.; Zhao, M.-Q.; Shpigel, N.; Levi, M. D.; Halim, J.; Taberna, P.; Barsoum, M.; Simon, P.; Gogotsi, Y. Ultra-High-Rate Pseudocapacitive Energy Storage in Two-Dimensional Transition Metal Carbides. *Nat. Energy* **2017**, *2*, 17105.
(43) Anwer, S.; Anjum, D. H.; Luo, S.; Abbas, Y.; Li, B.; Iqbal, S.; Liao, K. 2D $Ti_3C_2T_x$ MXene Nanosheets Coated Cellulose Fibers Based 3D Nanostructures for Efficient Water Desalination. *Chem. Eng. J.* **2021**, *406*, 126827.
(44) Liao, L.; Jiang, D.; Zheng, K.; Zhang, M.; Liu, J. Industry-Scale and Environmentally Stable $Ti_3C_2T_x$ MXene Based Film for Flexible Energy Storage Devices. *Adv. Funct. Mater.* **2021**, *31*, 2103960.
(45) Shayesteh Zeraati, A.; Mirkhani, S. A.; Sun, P.; Naguib, M.; Braun, P. V.; Sundararaj, U. Improved Synthesis of $Ti_3C_2T_x$ MXenes Resulting in Exceptional Electrical Conductivity, High Synthesis Yield, and Enhanced Capacitance. *Nanoscale* **2021**, *13*, 3572-3580.
(46) Yang, X.; Wang, Q.; Zhu, K.; Ye, K.; Wang, G.; Cao, D.; Yan, J. 3D Porous Oxidation-Resistant MXene/Graphene Architectures Induced by In Situ Zinc Template toward High-Performance Supercapacitors. *Adv. Funct. Mater.* **2021**, *31*, 2101087.
(47) Kshetri, T.; Khumujam, D. D.; Singh, T. I.; Lee, Y. S.; Kim, N. H.; Lee, J. H. Co-MOF@MXene-Carbon Nanofiber-Based Freestanding Electrodes for a Flexible and Wearable Quasi-Solid-State Supercapacitor. *Chem. Eng. J.* **2022**, *437*, 135338.
(48) Wang, Y.; Chen, N.; Liu, Y.; Zhou, X.; Pu, B.; Qing, Y.; Zhang, M.; Jiang, X.; Huang, J.; Tang, Q.; Zhou, B.; Yang, W. MXene/Graphdiyne Nanotube Composite Films for Free-Standing and Flexible Solid-State Supercapacitor. *Chem. Eng. J.* **2022**, *450*, 138398.
(49) Zhou, J.; Kang, Q.; Xu, S.; Li, X.; Liu, C.; Ni, L.; Chen, N.; Lu, C.; Wang, X.; Peng, L.; Guo, X.; Ding, W.; Hou, W. Ultrahigh Rate Capability of 1D/2D Polyaniline/Titanium Carbide (MXene) Nanohybrid for Advanced Asymmetric Supercapacitors. *Nano Res.* **2022**, *15*, 285-295.
(50) Liu, S.; Kang, L.; Hu, J.; Jung, E.; Henzie, J.; Alowasheeir, A.; Zhang, J.; Miao, L.;

Yamauchi, Y.; Jun, S. C. Realizing Superior Redox Kinetics of Hollow Bimetallic Sulfide Nanoarchitectures by Defect-Induced Manipulation toward Flexible Solid-State Supercapacitors. *Small* **2022**, *18*, 2104507.
(51) Wang, J.; Polleux, J.; Lim, J.; Dunn, B. Pseudocapacitive Contributions to Electrochemical Energy Storage in TiO_2 (Anatase) Nanoparticles. *J. Phys. Chem. C* **2007**, *111*, 14925-14931.
(52) Zhang, M.; Liang, R.; Yang, N.; Gao, R.; Zheng, Y.; Deng, Y. P.; Hu, Y.; Yu, A.; Chen, Z. Eutectic Etching toward In-Plane Porosity Manipulation of Cl-Terminated MXene for High-Performance Dual-Ion Battery Anode. *Adv. Energy Mater.* **2022**, *12*, 2102493.
(53) Yoon, Y.; Lee, M.; Kim, S. K.; Bae, G.; Song, W.; Myung, S.; Lim, J.; Lee, S. S.; Zyung, T.; An, K. A Strategy for Synthesis of Carbon Nitride Induced Chemically Doped 2D MXene for High-Performance Supercapacitor Electrodes. *Adv. Energy Mater.* **2018**, *8*, 1703173.
(54) Li, Y.; Wang, G.; Wei, T.; Fan, Z.; Yan, P. Nitrogen and Sulfur Co-Doped Porous Carbon Nanosheets Derived from Willow Catkin for Supercapacitors. *Nano Energy* **2016**, *19*, 165-175.
(55) Yan, J.; Ren, C. E.; Maleski, K.; Hatter, C. B.; Anasori, B.; Urbankowski, P.; Sarycheva, A.; Gogotsi, Y. Flexible MXene/Graphene Films for Ultrafast Supercapacitors with Outstanding Volumetric Capacitance. *Adv. Funct. Mater.* **2017**, *27*, 1701264.
(56) Liu, W.; Wang, Z.; Su, Y.; Li, Q.; Zhao, Z.; Geng, F. Molecularly Stacking Manganese Dioxide/Titanium Carbide Sheets to Produce Highly Flexible and Conductive Film Electrodes with Improved Pseudocapacitive Performances. *Adv. Energy Mater.* **2017**, *7*, 1602834.
(57) Wei, Y.; Zheng, M.; Luo, W.; Dai, B.; Ren, J.; Ma, M.; Li, T.; Ma, Y. All Pseudocapacitive MXene-MnO_2 Flexible Asymmetric Supercapacitor. *J. Energy Storage* **2022**, *45*, 103715.
(58) Yang, L.; Zheng, W.; Zhang, P.; Chen, J.; Tian, W. B.; Zhang, Y. M.; Sun, Z. M. MXene/CNTs Films Prepared by Electrophoretic Deposition for Supercapacitor Electrodes. *J. Electroanal. Chem.* **2018**, *830-831*, 1-6.
(59) Zhang, P.; Zhu, Q.; Soomro, R. A.; He, S.; Sun, N.; Qiao, N.; Xu, B. In Situ Ice Template Approach to Fabricate 3D Flexible MXene Film-Based Electrode for High Performance Supercapacitors. *Adv. Funct. Mater.* **2020**, *30*, 2000922.
(60) Li, Z.; Dall'Agnese, Y.; Guo, J.; Huang, H.; Liang, X.; Xu, S. Flexible Freestanding All-MXene Hybrid Films with Enhanced Capacitive Performance for Powering a Flex Sensor. *J. Mater. Chem. A* **2020**, *8*, 16649-16660.
(61) Xu, S.; Li, Z.; Wei, G.; Wang, Y.; Yang, Y. Intercalation and Surface Modification of Two-Dimensional Transition Metal Carbonitride Ti_3CNT_x for Ultrafast Supercapacitors. *J. Mater. Chem. A* **2022**, *10*, 18812-18821.
(62) Cai, M.; Wei, X.; Huang, H.; Yuan, F.; Li, C.; Xu, S.; Liang, X.; Zhou, W.; Guo, J. Nitrogen-Doped $Ti_3C_2T_x$ MXene Prepared by Thermal Decomposition of Ammonium Salts and Its Application in Flexible Quasi-Solid-State Supercapacitor. *Chem. Eng. J.* **2023**, *458*, 141338.

1 For Table of Contents Only

2